

Diagnosing Unmodeled Neutrino Physics via DUNE and T2HK Complementarity

João Paulo Pinheiro ^{1,2, a} and Ushak Rahaman ^{3, b}

¹*State Key Laboratory of Dark Matter Physics, Tsung-Dao Lee Institute & School of Physics and Astronomy, Shanghai Jiao Tong University, Shanghai 200240, China*

²*Key Laboratory for Particle Astrophysics and Cosmology (MOE) & Shanghai Key Laboratory for Particle Physics and Cosmology, Shanghai Jiao Tong University, Shanghai 200240, China*

³*Tata Institute of Fundamental Research, Homi Bhabha Road, Colaba, Mumbai 400005, India*

(Dated: March 17, 2026)

Unmodeled beyond Standard Model (BSM) physics in neutrino propagation can masquerade as parameter degeneracies in future precision measurements. Because the upcoming DUNE and T2HK experiments will operate at substantially different baselines, interpreting their data under the standard three-flavor framework provides a powerful diagnostic tool: any propagation BSM effect will inevitably manifest as an artificial tension between their extracted parameters. We demonstrate this principle using the complex non-standard interactions (NSI) currently favored to resolve the $\sim 2\sigma$ tension between $\text{NO}\nu A$ and T2K. If these NSI solutions are realized, the NSI-induced interference term $\propto \sin(\delta_{\text{CP}} + \phi)$ systematically distorts the DUNE appearance rates, leading to a correlated misidentification of the atmospheric mixing octant and the CP phase δ_{CP} . Specifically, for $\varepsilon_{e\mu}$ ($\varepsilon_{e\tau}$) NSI, the DUNE fit shifts toward CP-conserving values (the opposite CP half-plane) along with a preference for the wrong octant. In contrast, the shorter-baseline T2HK experiment remains largely insensitive to this effect. The resulting $\sim 3\sigma$ incompatibility between the DUNE and T2HK standard-fit results (after 6 years of data collection for each experiment) provides a robust experimental diagnostic for propagation NSI, illustrating how baseline complementarity is essential to uncover new physics in the precision era.

Introduction: Neutrino oscillation physics has entered the precision era. Recent results from JUNO [1] have determined the solar oscillation parameters with unprecedented accuracy and, when combined with global oscillation data, show a preference for the normal mass ordering (NO)[2, 3]. Cosmological measurements of baryon acoustic oscillations by CMB[4] and DESI [5, 6] further disfavour the inverted ordering. With the mass ordering picture becoming clearer, two key unknowns remain: the octant of the atmospheric mixing angle θ_{23} and the value of the Dirac CP phase δ_{CP} .

The upcoming Deep Underground Neutrino Experiment (DUNE) [7] ($L = 1300$ km) and the Tokai-to-Hyper-Kamiokande (T2HK) experiment [8] ($L = 295$ km) are designed to determine these remaining parameters with unprecedented precision through the $\nu_{\mu} \rightarrow \nu_e$ appearance channel. However, as we enter this high-precision regime, unmodeled beyond Standard Model (BSM) physics in neutrino propagation poses a critical challenge: it can easily masquerade as standard parameter degeneracies. Because DUNE and T2HK operate at drastically different baselines, their corresponding matter effects differ significantly. Consequently, any unmodeled BSM propagation effect will modify their appearance probabilities differently. Fitting their combined future data under the strict assumption of standard three-flavor oscillations would inevitably generate an artificial tension between the parameters inferred by each experiment. This baseline complementarity, therefore, transforms the combination

of DUNE and T2HK into a unique, generalized diagnostic tool for new physics.

To concretely demonstrate this diagnostic capability, we can look to the current generation of long-baseline experiments for a highly motivated BSM test case. The T2K [9] ($L = 295$ km) and $\text{NO}\nu A$ [10] ($L = 810$ km) experiments currently provide the leading measurements of the appearance channel, but they exhibit a mild but persistent inconsistency under the assumption of normal ordering. T2K observes a large neutrino–antineutrino appearance asymmetry consistent with near-maximal CP violation ($\delta_{\text{CP}} \simeq -\pi/2$), whereas $\text{NO}\nu A$ measures a smaller asymmetry than expected for this value of δ_{CP} . Because matter effects enhance the asymmetry at $\text{NO}\nu A$ relative to T2K under NO, the two results cannot be simultaneously accommodated within the standard three-flavor framework, leading to a $\sim 2\sigma$ tension [11–15].

A compelling explanation for this discrepancy is provided by neutral-current non-standard interactions (NSI) during propagation [16–19]. Complex off-diagonal NSI introduce additional phases in the matter potential, generating a new interference term in the oscillation probability. Because this contribution grows with baseline and neutrino energy, it affects $\text{NO}\nu A$ more strongly than T2K and can reconcile the two current data sets while preserving normal ordering[20–27].

In this work, we adopt these specific propagation NSI solutions as a realistic proxy for generic unmodeled new physics. We show that if these solutions are realized in nature, a standard analysis of DUNE measurements simultaneously misidentifies the octant of θ_{23} and the value of δ_{CP} . The two biases are correlated, arising from the same NSI-induced CP-odd interference term in the

^a joapaulo.pinhoiro@sjtu.edu.cn

^b ushak.rahaman@cern.ch

appearance probability. In contrast, the shorter-baseline T2HK experiment is largely insensitive to this propagation effect. Consequently, the standard-fit results of DUNE and T2HK become incompatible, yielding a 3.3–3.4 σ tension in a parameter-goodness-of-fit test, after 6 years of data collection for each experiment. This robust discordance illustrates exactly how baseline complementarity can act as an experimental diagnostic for new physics in the precision era.

NO ν A–T2K tension and NSI as a resolution: As outlined above, the current discrepancy between NO ν A and T2K serves as an ideal test case for how differing matter effects can expose unmodeled propagation physics. To understand the mechanics of this tension, we note that the most important observable governing both δ_{CP} and the mass ordering in long-baseline experiments is the matter–antimatter appearance asymmetry

$$A_{CP} \equiv P(\nu_\mu \rightarrow \nu_e) - P(\bar{\nu}_\mu \rightarrow \bar{\nu}_e). \quad (1)$$

T2K observes a large positive asymmetry consistent with near-maximal CP violation ($\delta_{CP} \simeq -\pi/2$). Under normal ordering (NO), matter effects enhance this asymmetry at the longer-baseline NO ν A experiment. Consequently, the standard framework predicts a larger asymmetry in NO ν A if the T2K result is interpreted as $\delta_{CP} \simeq -\pi/2$. Instead, NO ν A measures a smaller asymmetry, leading to the aforementioned $\sim 2\sigma$ tension between the two experiments under NO [11–15].

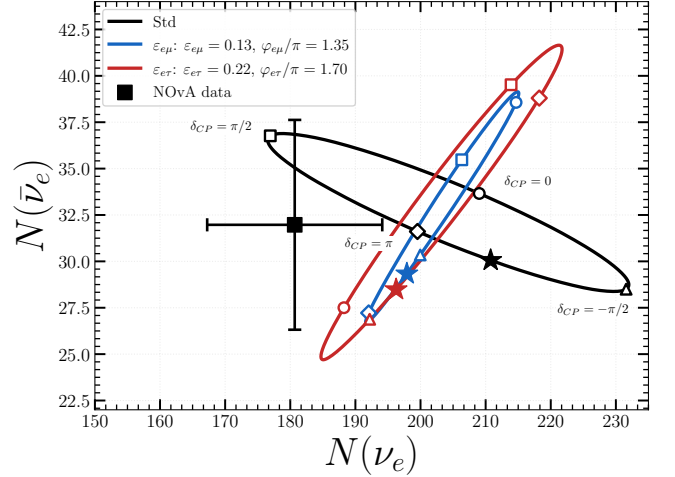
This feature can be understood from the perturbative expansion of the $\nu_\mu \rightarrow \nu_e$ appearance probability in matter [28, 29]. The standard probability can be written as $P_{\text{std}} = P_0 + P_1$, where the leading atmospheric term $P_0 \simeq 4s_{13}^2 s_{23}^2 f^2$ (with $f = \sin[(1 - \hat{A})\hat{\Delta}]/(1 - \hat{A})$ a matter-modified oscillation function, the dimensionless term $\hat{A} = 2EV_{CC}/\Delta_{31}$, where $V_{CC} = \sqrt{2}G_F n_e$, with G_F the Fermi constant and n_e the electron density in Earth matter, and $\hat{\Delta} = \Delta_{31}L/(4E)$) carries no CP phase, while the interference term P_1 contains $\cos(\hat{\Delta} + \delta_{CP})$. Under $\nu \leftrightarrow \bar{\nu}$ both \hat{A} and δ_{CP} change sign, yielding an asymmetry

$$A_{CP}^{\text{std}} \approx 16J_r \frac{\alpha}{\Delta_{31}} \Delta_{31} \sin^2 \hat{\Delta} \sin \delta_{CP} + A_{\text{mat}}(\hat{A}, \hat{\Delta}), \quad (2)$$

where A_{mat} denotes the purely matter-induced contribution. For NO this term has the same sign as the CP contribution, so the predicted asymmetry at NO ν A is generically larger than that at T2K. As illustrated in Fig. 1, the standard bi-event ellipses therefore fail to simultaneously reproduce the observed event counts of the two experiments. A natural explanation of this discrepancy is provided by neutral-current non-standard interactions (NSI) in neutrino propagation [20, 22–26, 30]. Such effects arise from dimension-six operators

$$\mathcal{L}_{\text{NSI}} = -2\sqrt{2}G_F \varepsilon_{\alpha\beta}^{fC} (\bar{\nu}_\alpha \gamma^\mu P_L \nu_\beta) (\bar{f} \gamma_\mu P_C f), \quad (3)$$

NO ν A ($L = 810$ km)



T2K ($L = 295$ km)

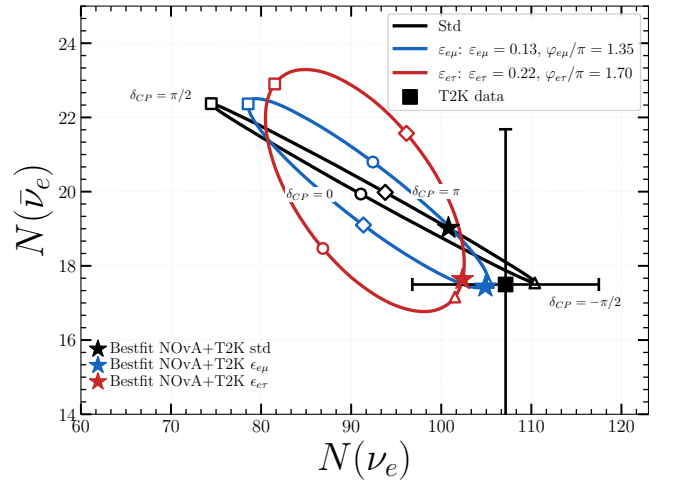


FIG. 1. Bi-event plot for NO ν A (upper) and T2K (lower). The ellipses are obtained by varying δ_{CP} over $[-\pi, \pi]$ with all other oscillation parameters fixed at the combined best-fit[3]. The data points are represented by black squares and the predicted number of events are represented as stars. The circle, square, diamond and triangle shapes represents $\delta_{CP} = 0, \pi/2, \pi(-\pi)$ and $-\pi/2$ respectively.

which modify the matter potential in the flavor basis,

$$H = H_{\text{vac}} + V_{CC} \begin{pmatrix} 1 + \varepsilon_{ee} & \varepsilon_{e\mu} & \varepsilon_{e\tau} \\ \varepsilon_{e\mu}^* & \varepsilon_{\mu\mu} & \varepsilon_{\mu\tau} \\ \varepsilon_{e\tau}^* & \varepsilon_{\mu\tau}^* & \varepsilon_{\tau\tau} \end{pmatrix}, \quad (4)$$

with effective parameters

$$\varepsilon_{\alpha\beta} = \sum_{f \in \{e, u, d\}} \frac{n_f}{n_e} \varepsilon_{\alpha\beta}^f. \quad (5)$$

For the Earth's crust [31],

$$\frac{n_u}{n_e} = 2 + Y_n \simeq 3.05, \quad \frac{n_d}{n_e} = 1 + 2Y_n \simeq 3.10. \quad (6)$$

The off-diagonal couplings are generally complex, $\varepsilon_{\alpha\beta} = |\varepsilon_{\alpha\beta}|e^{i\phi_{\alpha\beta}}$.

In the presence of $\varepsilon_{e\mu}$ or $\varepsilon_{e\tau}$, the appearance probability can be written as

$$P_{\mu e}^{\text{std+NSI}} = P_0 + P_1 + P_2, \quad (7)$$

where the standard terms are

$$P_0 \simeq 4s_{13}^2 s_{23}^2 f^2, \quad (8)$$

$$P_1 \simeq 8s_{13}s_{12}c_{12}s_{23}c_{23}\alpha f g \cos(\hat{\Delta} + \delta_{\text{CP}}), \quad (9)$$

and the NSI contribution is

$$P_2 \simeq 8s_{13}s_{23}\hat{A}|\varepsilon| \left[a f^2 \cos(\delta_{\text{CP}} + \phi) + b f g \cos(\hat{\Delta} + \delta_{\text{CP}} + \phi) \right], \quad (10)$$

where $\alpha = \frac{\Delta_{21}}{\Delta_{31}}$, and $g = \frac{\sin(\hat{A}\hat{\Delta})}{\hat{A}}$. The NSI coupling is parametrized as $\varepsilon_{e\mu} = |\varepsilon_{e\mu}|e^{i\phi_{e\mu}}$, with $a = \sin^2\theta_{23}$ and $b = \cos^2\theta_{23}$. For $\varepsilon_{e\tau} = |\varepsilon_{e\tau}|e^{i\phi_{e\tau}}$, the structure of Eq. 10 remains the same, but the coefficients become $a = s_{23}c_{23}$ and $b = -s_{23}c_{23}$, while all other terms remain unchanged. The antineutrino probability $P_{\bar{\mu}\bar{e}}$ is obtained by reversing the signs of \hat{A} , δ_{CP} , and ϕ . The new term P_2 modifies both the total appearance probability and the neutrino–antineutrino asymmetry. In particular, the asymmetry receives an additional contribution

$$\Delta A_{\text{CP}}^{\text{NSI}} \propto \hat{A} a |\varepsilon| \sin(\delta_{\text{CP}} + \phi), \quad (11)$$

introducing an effective CP phase ($\delta_{\text{CP}} + \phi$). Because $P_2 \propto \hat{A}|\varepsilon|$, the NSI effect grows with baseline and energy and therefore impacts NO ν A more strongly than T2K. As illustrated in Fig. 1, the off-diagonal NSI benchmarks shift the predicted event rates toward the observed values, allowing both data sets to be simultaneously accommodated.

Throughout this work we adopt the benchmark solutions obtained from the combined NO ν A+T2K analysis of Ref. [22, 24], summarized in Table I. These values lie within the ranges allowed by global oscillation analyses including complex NSI couplings [32, 33].

Importantly, the same NSI that reconcile the present data modify the appearance probability at future experiments. At the longer-baseline DUNE experiment the P_2 contribution is further enhanced, altering both the appearance rate and the CP asymmetry. Consequently, a standard three-flavor analysis of DUNE data would misidentify both the octant of θ_{23} and the value of δ_{CP} . We now study this effect quantitatively.

Implications for DUNE: The Deep Underground Neutrino Experiment (DUNE) [7], with a baseline of 1300 km, is designed to disentangle CP violation from matter effects and determine the remaining oscillation parameters with high precision. Owing to its longer baseline and higher neutrino energies compared to T2K and NO ν A, matter effects play a significantly larger role.

	Benchmark 1	Benchmark 2
NSI coupling	$\varepsilon_{e\mu}$	$\varepsilon_{e\tau}$
$ \varepsilon $	0.13	0.22
ϕ [°]	1.35	1.70
$\sin^2\theta_{23}^{\text{true}}$	0.56	0.56
$\delta_{\text{CP}}^{\text{true}}$ [°]	-0.56	-0.58

TABLE I. NSI benchmark points adopted in this work, corresponding to the best-fit solutions found in a combined analysis of NO ν A and T2K data under the NO hypothesis [22, 24]. Both points reconcile the NO ν A–T2K tension via off-diagonal propagation NSI.

Acting as a concrete proxy for generic propagation new physics, we study how the NSI solutions that reconcile the NO ν A–T2K tension would affect the interpretation of DUNE data if analyzed strictly within the standard three-flavor framework. True spectra are generated with NSI using the benchmark parameters of Table I, while the test spectra assume standard oscillations. Simulations are performed with the GLoBES framework [34, 35] using the official DUNE configuration: a 40 kt liquid-argon detector, a 1.2 MW beam at 120 GeV, and 3.5 + 3.5 years of neutrino and antineutrino running, corresponding to ~ 300 kt · MW · yr. Systematic uncertainties are included through Gaussian pulls following the DUNE TDR prescription [36]. The true oscillation parameters are $\sin^2\theta_{23} = 0.56$ and $\delta_{\text{CP}} \simeq -\pi/2$ under NO.

The analysis simultaneously includes ν_e ($\bar{\nu}_e$) appearance and ν_μ ($\bar{\nu}_\mu$) disappearance channels. The disappearance channel mainly constrains $\sin^2 2\theta_{23}$ and $|\Delta m_{31}^2|$ through the survival probability $P(\nu_\mu \rightarrow \nu_\mu) \simeq 1 - \sin^2 2\theta_{23} \sin^2 \Delta_{31}$, which is symmetric under $\theta_{23} \rightarrow \pi/2 - \theta_{23}$ and therefore insensitive to the octant. Since the off-diagonal NSI parameters $\varepsilon_{e\mu}$ and $\varepsilon_{e\tau}$ enter the Hamiltonian only in the e – μ and e – τ sectors (*cf.* Eq. 4), their effect on disappearance probabilities is small. Consequently the dominant NSI impact arises from the appearance channel, leaving the determination of $|\Delta m_{31}^2|$ and $\sin^2 2\theta_{23}$ largely unaffected while preserving the octant–CP degeneracy generated by P_2 .

The upper panel of Fig. 2 shows the bi-probability plot for DUNE with $P_{\mu e}$ ($P_{\bar{\mu}\bar{e}}$) on the x (y) axis. For both NSI benchmarks, the NSI ellipse corresponding to θ_{23} in the higher octant overlaps substantially with the standard three-flavor ellipse for the lower octant. In benchmark 1 the true point lies directly on the LO standard ellipse, while in benchmark 2 it lies very close to it. Consequently, event rates generated with NSI and θ_{23} in HO can be reproduced by standard oscillations with θ_{23} in LO and a shifted δ_{CP} . The lower panel of Fig. 2 shows that the same degeneracy persists at the level of integrated event counts.

Although the analytical discussion below focuses on the oscillation maximum, the numerical analysis uses the full DUNE energy spectrum (~ 0.5 –8 GeV) with the

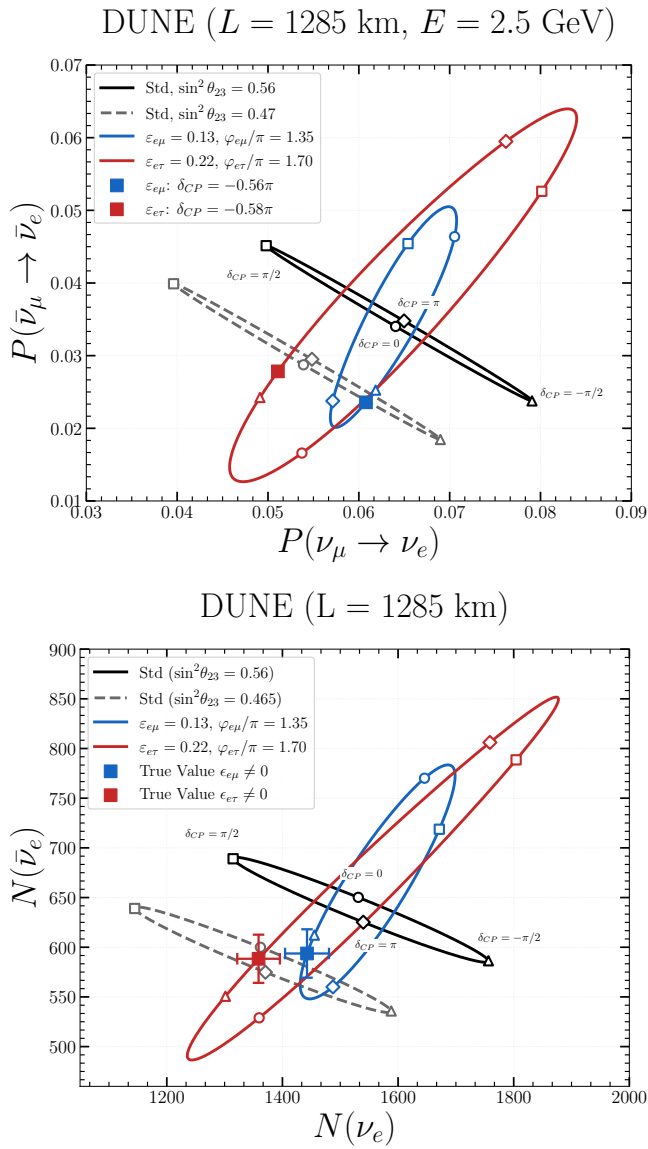


FIG. 2. Bi-probability plot (upper) and bi-event (lower) plot for DUNE. For both cases, the ellipses are obtained by varying δ_{CP} over $[-\pi, \pi]$ with all other oscillation parameters fixed at the combined best-fit [3]. The predicted probability and simulated data points use Benchmarks 1 and 2 from table I as references and are represented by colored squares. The black ellipse represents the standard prediction for the upper octant (UO), while the gray dashed ellipse represents the standard prediction for the lower octant (LO). The blue and red ellipses represent the prediction for non-zero NSIs suggested by benchmarks 1 and 2, respectively. The circle, square, diamond and triangle shapes represent $\delta_{CP} = 0, \pi/2, \pi(-\pi)$ and $-\pi/2$ respectively.

binning specified in the TDR [36]. The bi-event plots incorporate the flux, cross sections, and detector response. The close correspondence between the bi-probability and bi-event representations indicates that the degeneracy persists after spectral integration, since the P_2 contribution maintains the same sign and magnitude over the energy region dominating the event sample.

Analytically, for DUNE one obtains approximately, for eq. 10, $\hat{A} \simeq 0.22 [E/(2.5 \text{ GeV})]$, where 2.5 GeV corresponds to the first oscillation maximum. At the DUNE flux peak ($\hat{\Delta} \simeq \pi/2$), the dominant CP-odd contribution to the asymmetry $A_{CP} = P_{\mu e} - P_{\bar{\mu} \bar{e}}$ arises from P_1 (proportional to $\sin \delta_{CP}$) and from P_2 (proportional to $\sin(\delta_{CP} + \phi)$). The combination $(\delta_{CP} + \phi)$ therefore acts as an effective CP phase, $\delta_{CP}^{\text{eff}} = \delta_{CP} + \phi$. For benchmark 1, $\phi_{e\mu} = 1.35\pi$ and $\delta_{CP} \simeq -\pi/2$ give $\delta_{CP}^{\text{eff}} \simeq 0.85\pi$, close to the CP-conserving value π . In this case the NSI contribution suppresses the large asymmetry expected at maximal CP violation, and a standard oscillation fit compensates by shifting the inferred δ_{CP} toward CP-conserving values. For benchmark 2 ($\phi_{e\tau} = 1.70\pi$), $\delta_{CP}^{\text{eff}} \simeq 1.20\pi$ lies in the opposite half-plane, driving the fitted δ_{CP} across the CP-conserving boundary even though the true value is $\delta_{CP} \simeq -\pi/2$.

The coefficient a in Eq. 10 also determines the degree of octant misidentification. For $\varepsilon_{e\mu}$, $a = \sin^2 \theta_{23}$ distinguishes HO from LO, so the NSI ellipse in the bi-probability plane only partially overlaps with the LO ellipse of the standard scenario, producing a weaker octant degeneracy ($\sim 2\sigma$). In contrast, for $\varepsilon_{e\tau}$, $a = s_{23}c_{23} = \frac{1}{2} \sin 2\theta_{23}$ is symmetric under $\theta_{23} \rightarrow \pi/2 - \theta_{23}$, implying that P_2 alone cannot distinguish the two octants. This symmetry leads to an intrinsic octant degeneracy when both true and test event rates include NSI [37, 38].

Among the three terms in Eq. 7, the first two (P_0 and P_1) reproduce the standard oscillation probability $P_{\mu e}^{\text{std}}$. From Eqs. 8 and 9, $P_{\mu e}^{\text{std}}$ is maximized for normal ordering, $\delta_{CP} = -\pi/2$, and θ_{23} in the higher octant. The additional NSI term P_2 reduces this probability for the parameter region preferred by the combined NO ν A–T2K data, which favor $\pi < \phi < 2\pi$ at 1 σ C.L. In this region $\cos(\delta_{CP} + \phi) < 1$ for $\delta_{CP} = -90^\circ$, leading to a suppression of the ν_e (and also $\bar{\nu}_e$) appearance probability. Within the standard three-flavor framework this suppression can be accommodated by shifting the fitted value of θ_{23} from HO to LO and a shift in the fitted value of δ_{CP} . Since, the suppression in oscillation probability due to NSI is larger in case of $\varepsilon_{e\tau}$, to accommodate this shift in the fitting with standard oscillation scheme, the fitted δ_{CP} value needs to be shifted to the opposite half plane along with shifting the fitted octant of θ_{23} from HO to LO. Consequently, the wrong-octant solution at DUNE arises only for the specific combination of δ_{CP} and ϕ favored by the NO ν A–T2K data. For any other combination of ϕ and δ_{CP} , it was possible to remove the wrong octant solution in case of test event generated with standard oscillation scheme.

If a degeneracy occurs between $P_{\mu e}^{\text{std+NSI}}$ in HO and $P_{\mu e}^{\text{std}}$ in LO with a shifted CP phase δ'_{CP} , the condition reads

$$(P_0 + P_1 + P_2)_{\text{HO}, \phi, \delta_{CP}}^{\text{std+NSI}} = (P_0 + P_1)_{\text{LO}, \delta'_{CP}}^{\text{std}}. \quad (12)$$

At the DUNE flux peak ($\hat{\Delta} \simeq \pi/2$), and for the special case $\delta_{CP} = \delta'_{CP} = 0$, the P_1 term becomes negligible on

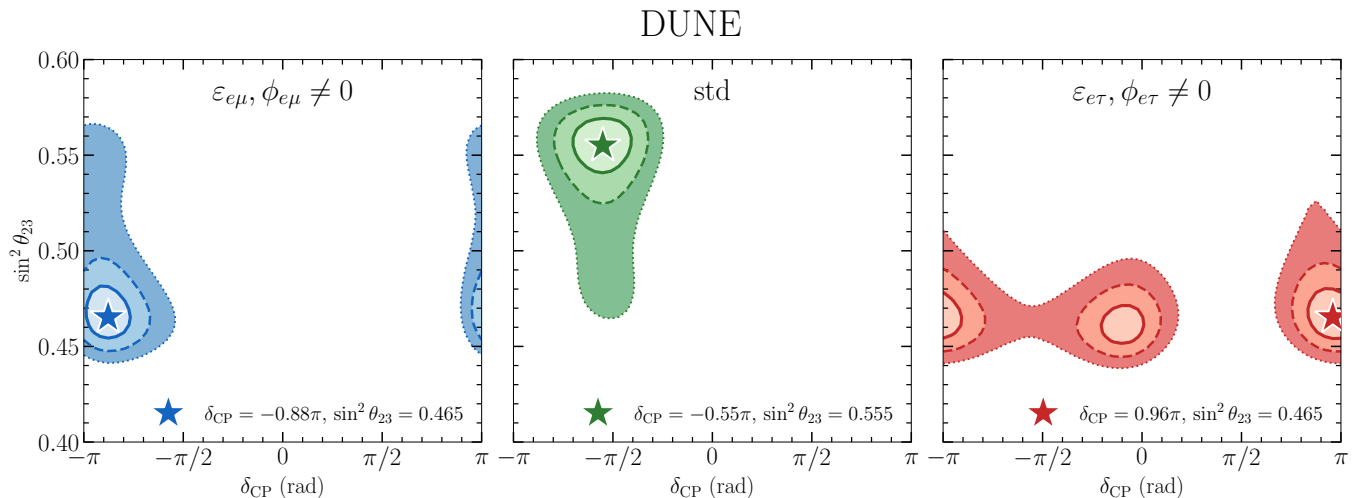


FIG. 3. Allowed regions in the $\sin^2 \theta_{23}$ - δ_{CP} plane from a standard three-flavor analysis of DUNE data. *Left*: The simulated data with true value driven by $\varepsilon_{e\mu}$ (benchmark 1); *center*: the simulated data with true value driven standard oscillations; *right*: the simulated data with true value driven by $\varepsilon_{e\tau}$ (benchmark 2). Contours at 1σ , 2σ and 3σ are shown. The star marks the best-fit point after analyzing the simulated data using standard oscillation.

both sides. Taking $|\varepsilon_{e\mu}| = 0.13$, Eq. 12 yields $\phi_{e\mu} \simeq 0.08\pi$ and 1.03π . Similar solutions exist for $\delta_{\text{CP}} \neq \delta'_{\text{CP}}$ and for NSI driven by $\varepsilon_{e\tau}$, confirming the generality of the degeneracy.

For antineutrinos the corresponding condition is

$$(\bar{P}_0 + \bar{P}_1 + \bar{P}_2)_{\text{HO},\phi,\delta_{\text{CP}}}^{\text{std+NSI}} = (\bar{P}_0 + \bar{P}_1)_{\text{LO},\delta'_{\text{CP}}}^{\text{std}}. \quad (13)$$

Solving Eqs. 12 and 13 determines the allowed values of ϕ and δ'_{CP} , where the ν_e and $\bar{\nu}_e$ appearance probabilities for NSI due to $\varepsilon_{e\mu}$ ($\varepsilon_{e\tau}$) with a fixed $\phi_{e\mu}$ ($\phi_{e\tau}$) and δ_{CP} , with θ_{23} in HO could be mimicked by standard oscillation probability with a δ'_{CP} and θ_{23} in LO.

The resulting allowed regions in the $\sin^2 \theta_{23}$ - δ_{CP} plane are shown in Fig. 3. In the standard case (center panel), DUNE correctly identifies the higher octant at $> 2\sigma$ and establishes near-maximal CP violation at $> 3\sigma$. In contrast, when the true spectra contain NSI, the interpretation changes qualitatively.

For benchmark 1 ($\varepsilon_{e\mu}$), the best-fit value shifts to $\delta_{\text{CP}} \simeq -0.88\pi$, close to CP conservation, while the higher octant becomes disfavored at $> 2\sigma$. For benchmark 2 ($\varepsilon_{e\tau}$), the distortion is stronger: the lower octant is preferred at $> 3\sigma$, and the fitted δ_{CP} becomes degenerate between 0 and π , recovering the true maximal phase only at 3σ .

In both cases the biases in θ_{23} and δ_{CP} arise from the same NSI contribution P_2 , which simultaneously modifies the total appearance rate and the CP asymmetry through the effective phase ($\delta_{\text{CP}} + \phi$). The distinct patterns visible in Fig. 3 could therefore help identify the underlying NSI scenario.

Previous work [37] showed that NSI can reduce DUNE's octant sensitivity when NSI effects are included in both true and test spectra. Here we consider the complementary situation in which NSI affect the true data but the analysis assumes the standard framework. In this case

DUNE can incorrectly prefer the *wrong* octant. While Ref. [38] predicted such a possibility for $\varepsilon_{e\tau}$ with $\delta_{\text{CP}} = 0$, our analysis shows that both $\varepsilon_{e\mu}$ and $\varepsilon_{e\tau}$ can induce correlated octant and CP-phase misidentification when the true phase is near maximal.

T2HK and DUNE-T2HK tension: We repeat the analysis for the Tokai-to-Hyper-Kamiokande (T2HK) experiment [8, 39, 40]. T2HK will send the upgraded J-PARC beam (4 MW) over a baseline of $L = 295$ km to a 500 kt fiducial Water Čerenkov detector. We assume an exposure of 3 yr ν + 3 yr $\bar{\nu}$ and simulate the experiment using GLOBES [34, 35] with the official configuration files. As in the DUNE analysis, the true spectra are generated with NSI at the benchmark values of Table I, while the fit assumes standard oscillations. The free parameters in the χ^2 minimization are $|\Delta m_{31}^2|$, $\sin^2 \theta_{23}$, and δ_{CP} , with the solar parameters fixed.

The shorter baseline of T2HK leads to a much smaller matter potential. At the peak energy $E \simeq 0.6$ GeV, $\hat{A} \simeq 0.05$, about four times smaller than at DUNE ($\hat{A} \simeq 0.22$ at $E \simeq 2.5$ GeV). Since the NSI term scales as $P_2 \propto \hat{A}|\varepsilon|$ [Eq. (10)], the NSI-induced shift of the bi-probability ellipse is correspondingly suppressed. As illustrated in Fig. 5, the NSI and standard ellipses lie close to each other, leaving little room for the octant-CP degeneracy observed at DUNE.

The resulting constraints in the $\sin^2 \theta_{23}$ - δ_{CP} plane are shown in Fig. 4. In the standard case (central panel), T2HK recovers the higher octant and near-maximal CP violation at high significance. For both NSI benchmarks the fit remains close to the true point: the higher octant is preferred at $> 2\sigma$ and the true phase $\delta_{\text{CP}} \simeq -0.55\pi$ is recovered within 1- 2σ . The best-fit δ_{CP} shifts only mildly ($\Delta\delta_{\text{CP}} \lesssim 0.1\pi$), and no degenerate lower-octant solution appears at 2σ .

T2HK

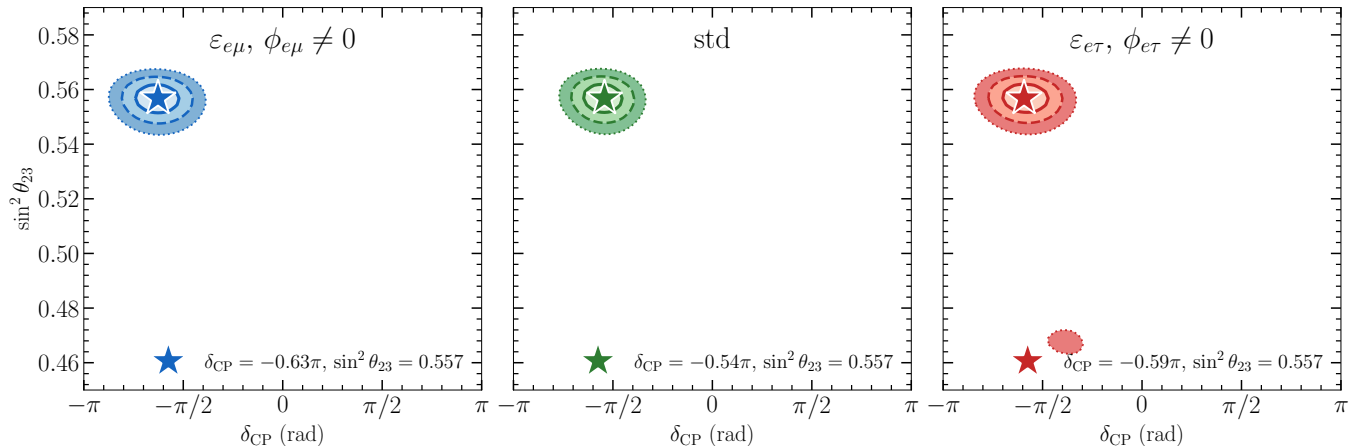


FIG. 4. Allowed regions in the $\sin^2 \theta_{23}$ - δ_{CP} plane from a standard three-flavor analysis of T2HK data. *Left*: The simulated data with true value driven by $\varepsilon_{e\mu}$ (benchmark 1); *center*: the simulated data with true value driven standard oscillations; *right*: the simulated data with true value driven by $\varepsilon_{e\tau}$ (benchmark 2). Contours at 1σ , 2σ and 3σ are shown. The star marks the best-fit point after analyzing the simulated data using standard oscillation.

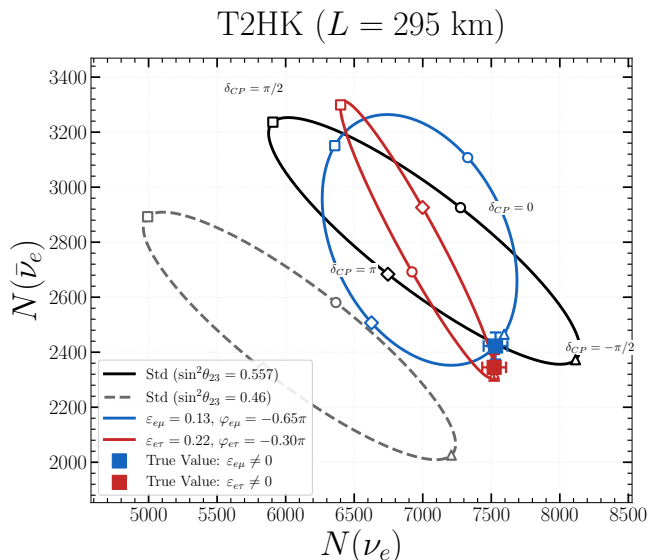


FIG. 5. Allowed regions in the $\sin^2 \theta_{23}$ - δ_{CP} plane from a standard three-flavor analysis of DUNE+T2HK data. *Left*: The simulated data with true value driven by $\varepsilon_{e\mu}$ (benchmark 1); *center*: the simulated data with true value driven standard oscillations; *right*: the simulated data with true value driven by $\varepsilon_{e\tau}$ (benchmark 2). Contours at 1σ , 2σ and 3σ are shown. The star marks the best-fit point after analyzing the simulated data using standard oscillation.

This robustness arises because the smaller matter effect suppresses the P_2 correction and the large T2HK statistics constrain the fit near the true parameters. The NSI benchmarks therefore do not significantly distort the T2HK inference, in sharp contrast to DUNE where the larger P_2 term drives the fit toward the wrong octant and a shifted CP phase.

Combined analysis: The contrasting responses of DUNE and T2HK [41] lead to tension when the two data sets are analyzed separately under the standard three-flavor hypothesis. The combined allowed regions are shown in Fig. 6. When the true spectra include NSI, DUNE favors a wrong-octant solution with shifted δ_{CP} , while T2HK recovers the true parameters. For the combined fit, in case of $\varepsilon_{e\mu}$ ($\varepsilon_{e\tau}$), T2HK + DUNE prefers HO (LO) for θ_{23} with δ_{CP} shifted slightly from the true value.

To quantify the inconsistency we apply the parameter goodness-of-fit (PG) test [42],

$$\chi_{\text{PG}}^2 = \min \left[\sum_i^N \chi_i^2 \right] - \sum_i^N \chi_{\text{min}, i}^2, \quad (14)$$

which follows a χ^2 distribution with $n = \sum_i n_i - n_{\text{glob}}$ degrees of freedom. We apply this test to the projected T2HK and DUNE data sets (appearance and disappearance channels in both neutrino and antineutrino modes) under NO, for case 1 (C1): fixing Δm_{21}^2 , θ_{12} , and θ_{13} to their best-fit values, so that each experiment depends on three parameters ($|\Delta m_{31}^2|$, $\sin^2 \theta_{23}$, δ_{CP}), giving $n = 3$ degrees of freedom, while for case 2 (C2): fixing Δm_{21}^2 and θ_{12} to their best-fit values, so that each experiment depends on three parameters ($|\Delta m_{31}^2|$, $\sin^2 \theta_{23}$, δ_{CP} , θ_{13}), giving $n = 4$ degrees of freedom. The true event spectra are generated with NSI at the benchmark values of Table I, while the fit is performed under the standard three-flavor hypothesis. The results are summarized in Table II.

Both benchmarks yield a T2HK + DUNE incompatibility at the $\sim 3\sigma$ level when interpreted within the standard three-flavor framework after 6 years of data taking, increasing the tension with more statistics. This

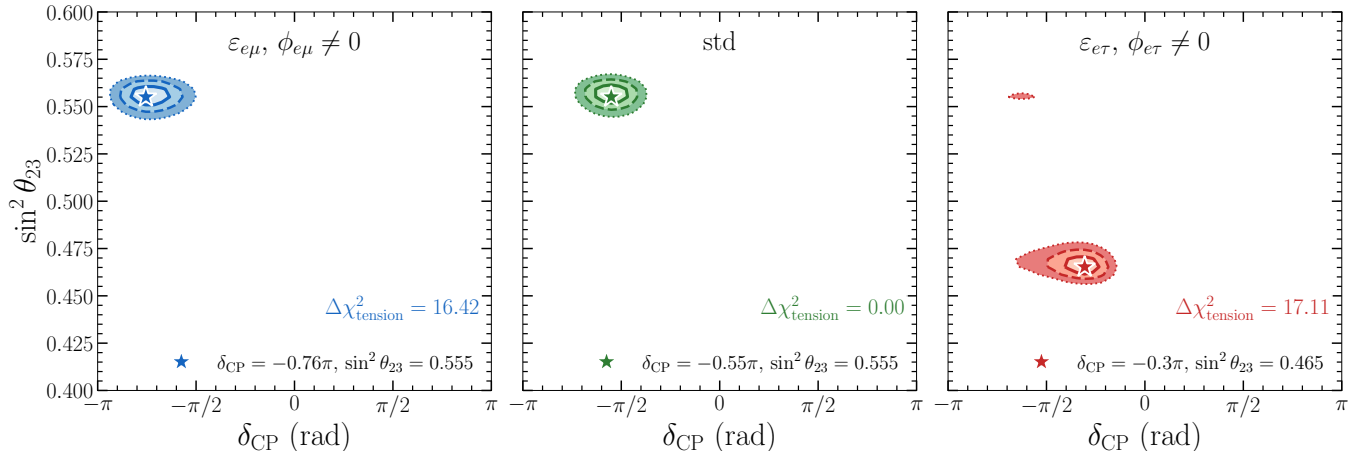
T2HK \oplus DUNE

FIG. 6. Allowed regions in the $\sin^2 \theta_{23}$ - δ_{CP} plane from a standard three-flavor analysis of T2HK \oplus DUNE data. *Left*: The simulated data with true value driven by $\varepsilon_{e\mu}$ (benchmark 1); *center*: the simulated data with true value driven standard oscillations; *right*: the simulated data with true value driven by $\varepsilon_{e\tau}$ (benchmark 2). Contours at 1σ , 2σ and 3σ are shown. The star marks the best-fit point after analyzing the simulated data using standard oscillation and the respective values of the $\Delta\chi^2$ to quantify the tension between the two experiments.

Cases	χ_{PG}^2/n	p -value	$\#\sigma$
C1: Benchmark 1 ($\varepsilon_{e\mu}$)	$16.42/(n=3)$	9.3×10^{-4}	3.3
C1: Benchmark 2 ($\varepsilon_{e\tau}$)	$17.11/(n=3)$	6.7×10^{-4}	3.4
C2: Benchmark 1 ($\varepsilon_{e\mu}$)	$16.42/(n=4)$	2.5×10^{-3}	3.0
C2: Benchmark 2 ($\varepsilon_{e\tau}$)	$17.11/(n=4)$	1.8×10^{-3}	3.1

TABLE II. Parameter goodness-of-fit test [42] for the consistency of T2HK and DUNE projected data under NO, assuming the standard oscillation framework. We consider two cases to quantify the tension, in case 1 (C1) the χ_{PG}^2 depends on three oscillation parameters. In case 2 (C2) the χ_{PG}^2 depends on four oscillation parameters. For more details, see the text.

arises from the baseline dependence of P_2 : T2HK, largely insensitive to propagation NSI, recovers the true oscillation parameters, whereas DUNE infers a shifted δ_{CP} and the wrong octant. The resulting discordance therefore provides a robust experimental diagnostic of new physics in the neutrino propagation sector.

Conclusion: In this letter, we have demonstrated that the baseline complementarity between future long-baseline experiments provides a powerful, generalized diagnostic tool for unmodeled new physics in neutrino propagation. Using the complex off-diagonal NSI—currently favored to resolve the $\sim 2\sigma$ NO ν A–T2K tension—as a highly predictive test case, we showed how such beyond Standard Model effects can masquerade as standard parameter degeneracies.

Because matter effects are significantly larger at DUNE, a standard three-flavor analysis of its data can simultaneously misidentify the octant of θ_{23} and the leptonic CP phase δ_{CP} . For $\varepsilon_{e\mu}$ NSI, the inferred δ_{CP} shifts toward

CP-conserving values while the higher octant becomes disfavored at 2σ , whereas for $\varepsilon_{e\tau}$ NSI, the fitted δ_{CP} can flip to the opposite half-plane together with a strong preference for the lower octant higher than 3σ . Both effects arise because the complex NSI phase ϕ modifies the CP asymmetry through the effective combination $\delta_{\text{CP}} + \phi$, leading to a large suppression of ν_e and $\bar{\nu}_e$ appearance probabilities that the standard fit erroneously accommodates by shifting to the lower octant. In contrast, T2HK is largely insensitive to these propagation effects owing to its shorter baseline, correctly recovering the true oscillation parameters.

The resulting mismatch between the DUNE and T2HK standard-fit results produces a 3.3 – 3.4σ inconsistency in a parameter goodness-of-fit test after 6 years of data collecting, getting increased with more statistics. This predicted tension between DUNE and T2HK is directly analogous to the current NO ν A–T2K discrepancy: in both cases, the tension arises because unmodeled propagation physics has a substantially stronger impact on the longer-baseline experiment.

While we have utilized NSI to quantitatively illustrate this effect, our findings establish a broader principle. If nature contains new physics in the neutrino propagation sector, assuming the standard hypothesis will force experiments with distinct matter effects to infer divergent parameters. Baseline complementarity between DUNE and T2HK therefore provides a robust and generic diagnostic: a future tension between their measurements of the octant or CP phase would be a compelling indication of BSM physics, with the current NO ν A–T2K discrepancy serving as a clear prelude to the degeneracies we must be prepared to disentangle.

Acknowledgment: We thank Shao-Feng Ge and Pe-

dro Machado for useful insights. JPP is supported by the National Natural Science Foundation of China (12425506 and 12375101). This work is also supported by State Key Laboratory of Dark Matter Physics. U.R. would like to acknowledge support from the Department of Atomic Energy, Government of India (Project Identification Number RTI 4002) and from the J. C. Bose Grant of the Anusandhan National Research Foundation (ANRF), Government of India (ANRF/JBG/2025/000265/PS). UR dedicates

this letter to Dr. Umar Khalid and Sharjeel Imam, who have been imprisoned in India without trial for more than five years. Their courage in standing by their convictions, even in the face of severe personal consequences, serves as a reminder of the importance of speaking truth to power. UR emphasizes that this dedication reflects solely his personal views. Neither the co-author of this paper nor the Tata Institute of Fundamental Research bears any responsibility for this statement.

-
- [1] A. Abusleme et al. (JUNO) (2025), 2511.14593.
- [2] I. Esteban, M. C. Gonzalez-Garcia, M. Maltoni, I. Martinez-Soler, J. P. Pinheiro, and T. Schwetz (2026), 2601.09791.
- [3] I. Esteban, M. C. Gonzalez-Garcia, M. Maltoni, I. Martinez-Soler, J. P. Pinheiro, and T. Schwetz, *JHEP* **12**, 216 (2024), 2410.05380.
- [4] N. Aghanim et al. (Planck), *Astron. Astrophys.* **641**, A6 (2020), [Erratum: *Astron. Astrophys.* 652, C4 (2021)], 1807.06209.
- [5] A. G. Adame et al. (DESI), *Astrophys. J.* **977**, 62 (2024), 2404.03002.
- [6] A. G. Adame et al. (DESI), *Astrophys. J.* **977**, 67 (2024), 2404.03000.
- [7] B. Abi et al. (DUNE) (2018), 1807.10334.
- [8] K. Abe et al. (Hyper-Kamiokande) (2018), 1805.04163.
- [9] Y. Itow et al. (T2K), in *3rd Workshop on Neutrino Oscillations and Their Origin (NOON 2001)* (2001), pp. 239–248, hep-ex/0106019.
- [10] D. S. Ayres et al. (NOvA) (2007).
- [11] M. A. Acero et al. (NOvA) (2021), 2108.08219.
- [12] J. Wolcott, *New oscillation results from nova with 10 years of data* (2024), talk given at the Neutrino 2024 meeting on June, 17th, 2024, URL <https://agenda.infn.it/event/37867/contributions/233955/attachments/121832/177712/2024-06-17%20Wolcott%20NOvA%202024%20results%20-%20NEUTRINO.pdf>.
- [13] K. Abe et al. (T2K Collaboration), *Phys.Rev.Lett.* **112**, 061802 (2014), 1311.4750.
- [14] K. Abe et al. (T2K Collaboration), *Phys.Rev.Lett.* **112**, 181801 (2014), 1403.1532.
- [15] S. Abubakar et al. (T2K, NOvA), *Nature* **646**, 818 (2025), 2510.19888.
- [16] L. Wolfenstein, *Phys. Rev. D* **17**, 2369 (1978).
- [17] S. P. Mikheyev and A. Y. Smirnov, *Sov. J. Nucl. Phys.* **42**, 913 (1985).
- [18] Y. Grossman, *Phys. Lett. B* **359**, 141 (1995), hep-ph/9507344.
- [19] *Neutrino Non-Standard Interactions: A Status Report*, vol. 2 (2019), 1907.00991.
- [20] L. S. Miranda, P. Pasquini, U. Rahaman, and S. Razzaque, *Eur. Phys. J. C* **81**, 444 (2021), 1911.09398.
- [21] X. Y. Yu, Z. Guan, U. Rahaman, and N. Ilic, *Nucl. Phys. B* **1023**, 117303 (2026), 2501.00146.
- [22] S. S. Chatterjee and A. Palazzo, *Phys. Rev. Lett.* **126**, 051802 (2021), 2008.04161.
- [23] U. Rahaman, S. Razzaque, and S. U. Sankar, *Universe* **8**, 109 (2022), 2201.03250.
- [24] S. S. Chatterjee and A. Palazzo (2024), 2409.10599.
- [25] P. B. Denton, J. Gehrlein, and R. Pestes, *Phys. Rev. Lett.* **126**, 051801 (2021), 2008.01110.
- [26] A. Cherchiglia, P. Pasquini, O. L. G. Peres, F. F. Rodrigues, R. R. Rossi, and E. S. Souza, *Phys. Rev. D* **112**, 093004 (2025), 2310.18401.
- [27] G. Alonso-Álvarez, J. M. Cline, B. Laurent, and U. Rahaman, *Eur. Phys. J. C* **85**, 635 (2025), 2407.13817.
- [28] A. Cervera, A. Donini, M. B. Gavela, J. J. Gomez Cadenas, P. Hernandez, O. Mena, and S. Rigolin, *Nucl. Phys. B* **579**, 17 (2000), [Erratum: *Nucl.Phys.B* 593, 731–732 (2001)], hep-ph/0002108.
- [29] M. Freund, *Phys. Rev. D* **64**, 053003 (2001), hep-ph/0103300.
- [30] U. Rahaman, *Eur. Phys. J. C* **81**, 792 (2021), 2103.04576.
- [31] A. M. Dziewonski and D. L. Anderson, *Phys. Earth Planet. Interiors* **25**, 297 (1981).
- [32] I. Esteban, M. C. Gonzalez-Garcia, M. Maltoni, I. Martinez-Soler, and J. Salvado, *JHEP* **08**, 180 (2018), [Addendum: *JHEP* 12, 152 (2020)], 1805.04530.
- [33] I. Esteban, M. C. Gonzalez-Garcia, and M. Maltoni, *JHEP* **06**, 055 (2019), 1905.05203.
- [34] P. Huber, M. Lindner, and W. Winter, *Comput. Phys. Commun.* **167**, 195 (2005), hep-ph/0407333.
- [35] P. Huber, J. Kopp, M. Lindner, M. Rolinec, and W. Winter, *Comput. Phys. Commun.* **177**, 432 (2007), hep-ph/0701187.
- [36] B. Abi et al. (DUNE) (2021), 2103.04797.
- [37] S. K. Agarwalla, S. S. Chatterjee, and A. Palazzo, *Phys. Lett. B* **762**, 64 (2016), 1607.01745.
- [38] J. Liao, D. Marfatia, and K. Whisnant, *Phys. Rev. D* **93**, 093016 (2016), 1601.00927.
- [39] K. Abe et al. (Hyper-Kamiokande Proto-Collaboration), *PTEP* **2015**, 053C02 (2015), 1502.05199.
- [40] Hyper-Kamiokande Collaboration, K. Abe, et al. (2018), 1805.04163.
- [41] R. Abdel Khaleq, J. L. Newstead, C. Simenel, and A. E. Stuchbery, *Phys. Rev. D* **111**, 033003 (2025), 2405.20060.
- [42] M. Maltoni and T. Schwetz, *Phys. Rev. D* **68**, 033020 (2003), hep-ph/0304176.